Canopy radiation transmission for an energy balance snowmelt model

Vinod Mahat[1] and David G. Tarboton[1]

Received 18 January 2011; revised 16 November 2011; accepted 25 November 2011; published 24 January 2012.

[1] To better estimate the radiation energy within and beneath the forest canopy for energy balance snowmelt models, a two stream radiation transfer model that explicitly accounts for canopy scattering, absorption and reflection was developed. Upward and downward radiation streams represented by two differential equations using a single path assumption were solved analytically to approximate the radiation transmitted through or reflected by the canopy with multiple scattering. This approximation results in an exponential decrease of radiation intensity with canopy depth, similar to Beer's law for a deep canopy. The solution for a finite canopy is obtained by applying recursive superposition of this two stream single path deep canopy solution. This solution enhances capability for modeling energy balance processes of the snowpack in forested environments, which is important when quantifying the sensitivity of hydrologic response to input changes using physically based modeling. The radiation model was included in a distributed energy balance snowmelt model and results compared with observations made in three different vegetation classes (open, coniferous forest, deciduous forest) at a forest study area in the Rocky Mountains in Utah, USA. The model was able to capture the sensitivity of beneath canopy net radiation and snowmelt to vegetation class consistent with observations and achieve satisfactory predictions of snowmelt from forested areas from parsimonious practically available information. The model is simple enough to be applied in a spatially distributed way, but still relatively rigorously and explicitly represent variability in canopy properties in the simulation of snowmelt over a watershed.

Citation: Mahat, V., and D. G. Tarboton (2012), Canopy radiation transmission for an energy balance snowmelt model, *Water Resour. Res.*, *48*, W01534, doi:10.1029/2011WR010438.

1. Introduction

[2] Snow accumulation, melt and sublimation processes are different for open and forest sites. Vegetation and land cover influences snow processes making it difficult to predict snowmelt which is responsible for water supply in much of the world, including the mountainous regions of the western U.S. where this study was conducted. The processes of snow accumulation and melt in open areas are understood for a range of climates and well represented in numerical models [*Anderson*, 1976; *Bartlett and Lehning*, 2002; *Jordan*, 1991; *Lehning et al.*, 2002; *Marks et al.*, 1992; *Price and Dunne*, 1976; *Tarboton and Luce*, 1996; *Wigmosta et al.*, 1994]. Prediction of the evolution of snow packs in forested areas is more complex [*Storck et al.*, 2002]. The forest canopy intercepts snow fall, attenuates radiation, and modifies the turbulent exchanges of energy and water vapor between snow in and under the canopy and the atmosphere, thereby affecting snow accumulation and melt. It is important for snowmelt models to be able to properly represent these processes so as to have correct sensitivity to canopy properties when they are used to address questions such as the impacts of climate and land cover changes on hydrologic response. Yet it is also important for models to not be overly complicated and demanding of input data. In this paper we address enhancements to the representation of canopy processes involved in the physically based modeling of energy balance processes of the snowpack.

[3] The purpose of this paper is to present and evaluate a relatively simple model to estimate beneath canopy radiation that drives the energy balance and snowmelt beneath the forest canopy. Parsimony in terms of model complexity and data requirements is a design consideration, striving for the best possible physical representations given commonly available data. The forest canopy is modeled as a single layer with parameters leaf area index and canopy cover fraction quantifying the radiation attenuation. A two stream radiation transfer model that explicitly accounts for canopy scattering, absorption and reflection is used. Upward and downward radiation streams represented by two differential equations using a single path assumption were solved analytically to approximate the radiation transmitted through or reflected by the canopy with multiple scattering. This approximation results in an exponential decrease of radiation intensity with canopy depth, similar to Beer's law for a deep canopy. In Beer's law solar radiation is decreased exponentially along the path through the absorbing medium

[1]Department of Civil and Environmental Engineering, Utah Water Research Laboratory, Utah State University, Logan, Utah, USA.

0043-1397/12/2011WR010438

without accounting for scattering [*Monteith and Unsworth*, 1990]. The solution for a finite canopy is obtained by applying recursive superposition of this two stream single path deep canopy solution. The parameters required are the same parameters that are used in Beer's law, but the theoretical foundation of the model has been improved in that multiple scattering and a finite canopy depth are represented.

[4] Radiation is the main driver of the energy balance and snowmelt. This paper focuses on how to represent the penetration of radiation through a forest canopy in an energy balance snowmelt model. The input of solar radiation to the ground surface whether in the open or beneath the canopy varies depending on solar angle and azimuth as well as cloudiness and topography (slope and aspect) [*Link et al.*, 2004; *Stähli et al.*, 2009]. Net radiation at the snow surface then depends on reflection from the surface, governed by the surface albedo as well as scattering and multiple reflections between the snow surface and canopy. Surface albedo depends on coverage by snow (coverage is patchy when the snow is shallow and surface rough), snow surface grain size which is related to age and the presence of dust or litter on the surface (how fresh and clean is the snow) [*Hardy et al.*, 2000; *Jordan*, 1991].

[5] A number of techniques have been used to model radiation beneath forest canopies. *Ellis and Pomeroy* [2007], *Essery et al.* [2003], *Koivusalo* [2002] and *Link and Marks* [1999] used Beer's law to attenuate the solar radiation penetrating a canopy. Depending on the density of the canopy, multiple scattering may increase the irradiance reaching the surface as compared to Beer's law, by up to 100% [*Nijssen and Lettenmaier*, 1999]. Efforts to develop simplified approaches to model radiation beneath the canopy accounting for multiple scattering of radiation include *Nijssen and Lettenmaier* [1999], *Tribbeck et al.* [2004], and *Yang et al.* [2001]. *Nijssen and Lettenmaier's* [1999] model provides a solution for infinitely deep canopy while *Tribbeck et al.*'s [2004] model assumes radiation scattered by the canopy is reflected equally in upward and downward directions and does not account for within canopy scattering. *Yang et al.* [2001] present a simplified two stream approach, but their model requires vegetation geometry information. The two path multiscattering approach we have taken accounts for multiscattering in a finite canopy more rigorously than these approaches, while not being more demanding of input data.

[6] *Dickinson* [1983] and *Sellers* [1985] developed a two stream approximation for radiation transfer through the atmosphere or a vegetation canopy which includes multiple scattering [*Dickinson*, 1983; *Sellers*, 1985]. In this two stream approximation, upward and downward diffuse solar is expressed using two differential equations quantifying the change in downward and upward radiation due to interception, absorption and scattering in a semi-infinite canopy. This approach applies to integrated quantities as opposed to angular-dependent intensities [*Meador and Weaver*, 1980] and neglects anisotropy that may result due to angular effects in scattering. *Roujean* [1996] also developed a tractable physical model of shortwave radiation interception by vegetative canopies. This accounted for direct transmittance, single and multiple scattering in a semi-infinite canopy. The approach we have developed here is closely based on the concepts from these papers but extended from a semi-infinite (deep) canopy to a finite canopy using recursive superposition. We have also integrated our approach into a snowmelt model so as to enhance the physically based modeling of energy balance processes of the snowpack in forested environments.

[7] A more detailed approach was taken by *Li et al.* [1995] and *Ni et al.* [1997] in the Geometric-optical and radiative transfer (GORT) model which accounts for the three dimensional geometry of the forest canopy and includes multiple scattering within and beneath the canopy. The GORT model is computationally expensive and also requires parameters such as crown geometry and foliage area volume density that are difficult to measure in the field [*Hardy et al.*, 2004]. There are also a number of other single or multiple-layer models in the literature [e.g., *Flerchinger and Yu*, 2007; *Flerchinger et al.*, 2009; *Norman*, 1979; *Zhao and Qualls*, 2005; 2006] that represent radiation transfer based on more detailed canopy information (e.g., leaf density, inclination, orientation, crown diameter and depth, etc.). Our approach has been developed to avoid dependence on this practically hard to obtain information.

[8] There is also work that has examined the heterogeneity of forested surfaces and brought in information on canopy fraction and tree shape to compute canopy radiation transmissivity [*Essery et al.*, 2008; *Hu et al.*, 2010; *Niu and Yang*, 2004]. In some cases hemispherical photographs have been used to determine the parameters involved [*Essery et al.*, 2008; *Hardy et al.*, 2004; *Hu et al.*, 2010]. While this is a promising line of investigation we have chosen to, at this point in time, evaluate a parsimonious parameterization of vegetation that does not require this detailed information.

[9] The new radiation component developed fills the need for a parsimonious, yet rigorous physically based capability for modeling radiation transfer through forested canopies as it drives the energy balance and melt of a snowpack. It has been designed to avoid over-parameterization that leads to problems with parameter estimation and validation in more complex models. There are very few models that can be used when input data are limited, and are transportable and applicable at different places with little calibration.

[10] The new radiation transfer approach was added to the Utah Energy Balance (UEB) snowmelt model [*Tarboton and Luce*, 1996; *Tarboton et al.*, 1995] to model snow energy and mass balances within and beneath the canopy driven by inputs of radiation and weather from above the canopy. The surface component retains the single layer parameterization of the original UEB model that focuses on surface mass and energy exchanges. It avoids the potential overparameterization that may result from attempting to represent the complexity of within snow processes using multiple layers. The added canopy component similarly uses a canopy parameterization that strives for a good physical representation of the processes involved without requiring hard to quantify information on canopy structure and leaf orientation.

2. Study Site

[11] Field measurements were carried out at the TW Daniel Experimental Forest (TWDEF) (available at http://danielforest.usu.edu) located about 30 miles North–East of

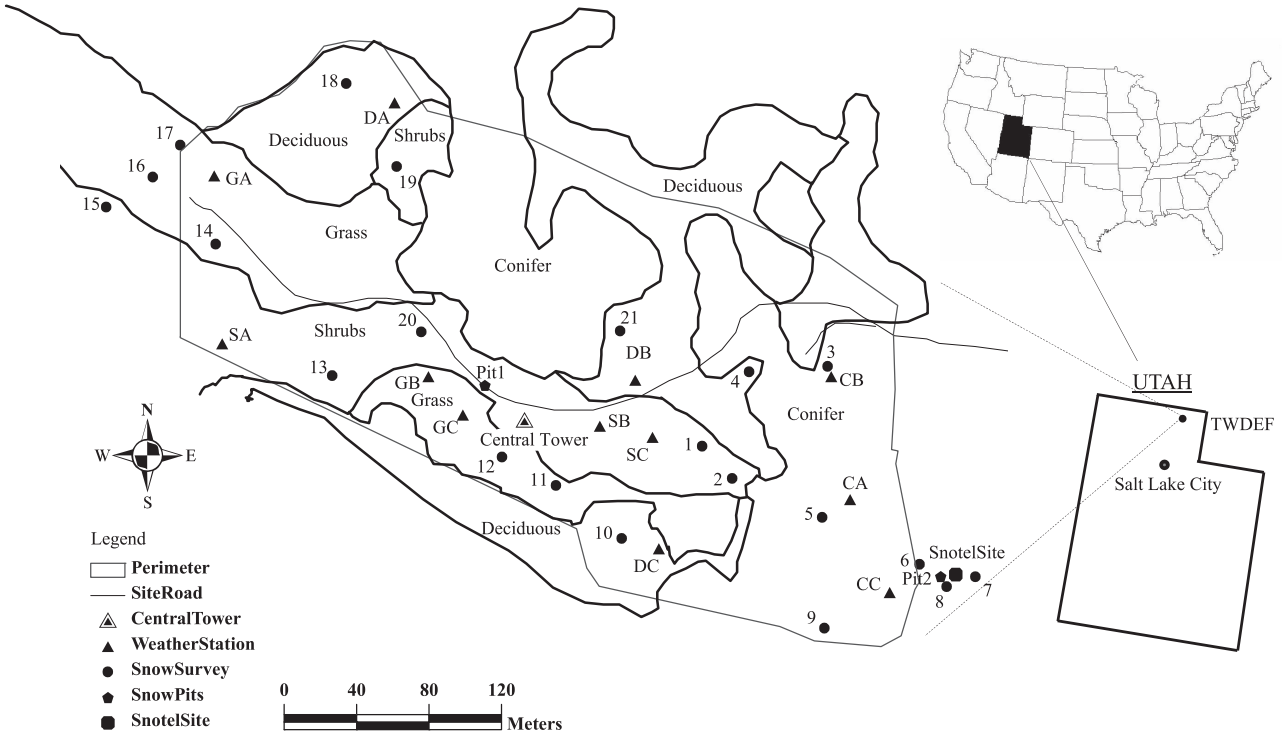

Figure 1. Site map of the TW Daniel Experimental Forest showing weather station towers, vegetation, survey points, pits and SNOTEL site.

Logan, Utah (Figure 1). TWDEF comprises an area of 0.78 km^2 at an elevation of approximately 2700 m. It lies at 41.86° North and 111.50° West. The TW Daniel Experimental Forest is on the divide of the watershed that contributes to the Logan River and Bear Lake. Average annual precipitation is about 950 mm of which about 80% is snow. The maximum snow depth can reach 5 m in the area where snow drifts occur. Vegetation is composed of deciduous forest (Aspen), coniferous forest (Engelmann spruce and subalpine fir), open meadows consisting of a mixture of grasses and forbs, and shrub areas dominated by sagebrush.

[12] Instrumentation was installed starting in 2006 to monitor weather and snow within four different vegetation classes: grass, shrubs, coniferous forest, and deciduous forest; and includes twelve weather station towers (three replicates in each vegetation class), one central tower (in shrub area) with more comprehensive radiation instrumentation and one SNOTEL station in a clearing within the coniferous forest. The following automated data were collected.

[13] 1. Continuous measurements of snow depth (Judd Communications depth sensor) at each of the twelve stations.

[14] 2. Continuous measurements of weather: temperature and humidity (Vaisala HMP50); wind (Met One, 014A); net radiation, (Kipp & Zonen NR-Lite) at one station in each vegetation class. These instruments were placed at heights above the ground of about 2.5 m in conifer, 4.5 m in deciduous and 4 m in shrub sites so as to remain above the deep snow that accumulates in the deciduous and shrubs areas.

[15] 3. Four separate radiation components: downward and upward shortwave and long wave (Hukseflux, NR01 four-way radiometer) and snow surface temperature (Apogee Instrument, IRR-PN) at the centralized weather station.

[16] 4. The standard suite of SNOTEL observations at the adjacent SNOTEL site, from which we used precipitation. This SNOTEL site was installed in summer 2007, so its data are first available for the 2007–2008 winter.

[17] Slope and aspect were determined from a 1 m resolution digital elevation model constructed from bare earth points classified from an airborne LiDAR survey of the site. Table 1 lists the site information, and in addition to these parameters includes parameters used with other aspects of the model that are not the focus of this paper.

[18] Field observations roughly every two weeks for four winters (2006–2007 to 2009–2010) comprised two snow pits: one in the shrub area (Pit 1, Figure 1) and the other in a conifer clearing (Pit 2, Figure 1), and snow depth at multiple locations in all four vegetation classes. Within each snow pit samples were taken at 10 cm vertical intervals over the entire snow pit depth using a 250 cm^3 stainless steel cutter to derive the snow density. The density measured at the pit in the shrub area was used to represent both

Table 1. Site Variables

Sites/Variables	Open	Deciduous	Conifer
Leaf area index	0.0	1	4.5
Canopy cover fraction	0.0	0.7	0.7
Canopy height (m)	0.0	15.0	15.0
Slope (degrees)	3.6	5.0	2.0
Aspect (degrees clockwise from N)	150	0.0	300
Latitude (degrees)	41.86	41.86	41.86
Branch interception capacity (kg m^{-2})	0.0	6.6	6.6
Average atmospheric pressure (Pa)	74,000	74,000	74,000

shrub and grass areas. Both shrub and grass are regarded as open because during the winter snow season snow completely covers the shrubs. Snow density measured in the conifer clearing was used to represent forested areas (both conifer and deciduous). These density values were used with the depth measurements at multiple locations to derive the snow water equivalent (SWE). Temperature was also measured at the surface and at 10 cm vertical intervals over the entire snow pit depth. These temperature measurements were used to derive the energy content of the snow. Numbered snow survey points (Figure 1) show locations where the depth measurements were made across the four vegetation classes.

3. Model Description

[19] The UEB snowmelt model [*Tarboton and Luce*, 1996] is a physically based point energy and mass balance model for snow accumulation and melt. Snowpack is characterized using three state variables, namely, snow water equivalent, W_s, (m), the internal energy of the snowpack and top layer of soil, U_s, (kJ m^{-2}), and the dimensionless age of the snow surface used for albedo calculations. The UEB model is a single layer model. U_s and W_s are predicted at each time step based on the energy balance. Details of the original UEB model formulation are given by *Tarboton et al.* [1995], *Tarboton and Luce* [1996] with enhancements for the calculation of surface temperature using a modified Force-Restore approach given by *Luce and Tarboton* [2010] and *You* [2004].

[20] In this paper we present the canopy radiation transmission component of an enhanced UEB model that includes representation of canopy processes. The canopy component is modeled as a single layer, which added to the original single layer UEB model results in a two-layer model that represents the surface and the canopy intercepted snow separately. Energy balances are solved iteratively for each layer to provide outputs of surface temperature, canopy temperature and the other energy fluxes that are based on canopy or surface temperature. The quantity and state of snow in the canopy is represented by a new state variable, canopy snow water equivalent, W_c (m). We assume that the energy content of intercepted snow in the canopy is negligible so canopy temperature, including snow in the canopy, is assumed to adjust to maintain energy equilibrium, except when this requires canopy temperature to be greater than freezing when snow is present in the canopy, in which case the extra energy drives the melting of snow in the canopy.

3.1. Shortwave Radiation

3.1.1. Partitioning of Radiation

[21] The incoming solar radiation reaching the canopy surface, Q_t (W m^{-2}) is partitioned into direct and diffuse components, Q_b (W m^{-2}) and Q_d (W m^{-2}), as these components penetrate the canopy separately. AT is the fraction of top of atmosphere total radiation reaching the top of the canopy either measured or estimated from diurnal temperature range using the procedure of *Bristow and Campbell* [1984]. This is split into direct radiation fraction, AT_b and diffuse radiation fraction AT_d. Cloudiness fraction, C_f, is estimated from AT using an the empirical relationship provided by *Shuttleworth* [1993]. We assume that when the sky is clear ($C_f = 0$) that a fraction λ of AT is direct. The value of λ may be estimated based on scattering and absorption properties of the cloud free atmosphere and is due to water vapor, dust and other scatterers in the atmosphere. We assume that when the sky is completely cloudy ($C_f = 1$) that all radiation is diffuse. Using these as boundary conditions and assuming linear variation of each factor with C_f (Figure 2) leads to

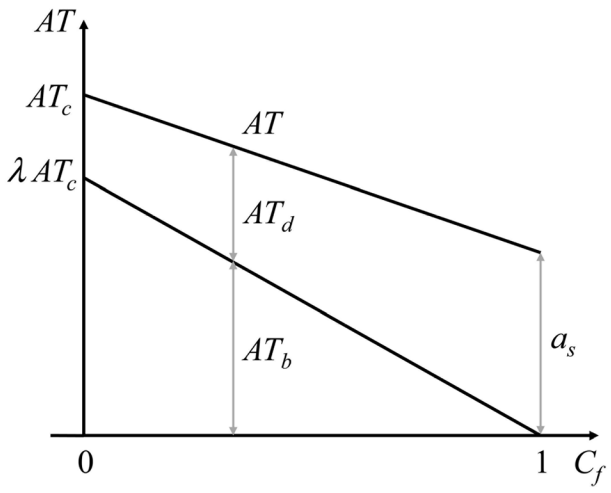

Figure 2. Partitioning of atmospheric transmission factor, AT into direct and diffuse components, AT_b and AT_d.

$$AT_b = \lambda AT_c(1 - C_f), \tag{1}$$

$$AT_d = AT - AT_b, \tag{2}$$

where $AT_c = \max(AT, a_s + b_s)$ is the clear sky transmission factor. $a_s + b_s$ is the fraction of extraterrestrial radiation reaching the surface on clear days. *Shuttleworth* [1993] recommended $a_s = 0.25$ and $b_s = 0.5$ for settings where no actual solar radiation data are available.

[22] Once AT_b and AT_d are estimated, the total incoming radiation can be partitioned into direct and diffuse parts

$$Q_b = \frac{AT_b}{AT} Q_t \tag{3}$$

$$Q_d = \frac{AT_d}{AT} Q_t. \tag{4}$$

3.1.2. Canopy Radiation Transmission

[23] We develop the canopy radiation transmission model in three steps. First the attenuation of incident radiation due to interception, but not scattering is quantified. This results in an exponential decrease of radiation intensity with depth into the canopy (Beer's law). Next we consider scattering using a two stream approach for an infinitely deep canopy. This results in a modified exponential attenuation. In the third step we consider a finite canopy with downward radiation incident at the top and upward radiation incident at the bottom. The direct and diffuse fractions of radiation transmitted through the canopy in the first step without scattering

are represented by τ_b'' and τ_d'', respectively. $\tau_b'^*$ and τ_d' denote the direct and diffuse fraction when there is scattering but for a deep canopy and τ_b and τ_d denote direct and diffuse fraction when there is scattering and the canopy is finite. The approach used is general such that it can be applied with both direct and diffuse radiation, and shortwave and longwave radiation, but with different scattering parameters. In this general approach we use Q to represent radiation that may be direct, Q_b, diffuse, Q_d, or longwave, Q_{li}, reaching the surface and Q_o to represent the corresponding the value of this incoming radiation at the top of the canopy (all radiation terms in W m^{-2}).

3.1.2.1. Radiation Transmission Without Scattering (Beer's Law)

[24] In considering the penetration of light through a canopy the interception of a beam at zenith angle θ by an incremental layer of vegetation results in reduction in intensity given by

$$dQ = -QG\rho\frac{dy}{\cos\theta}, \tag{5}$$

where Q is radiation intensity, ρ (m^{-1}) is the leaf density, y (m) is the distance measured vertically downward from the top of the canopy and G is a leaf orientation factor quantifying the average area of leaves when viewed from direction θ. Here G is assumed to be constant (i.e., independent of θ). Integrating equation (5) from the top of the canopy downward results in Beer's law (Figure 3)

$$Q = Q_o\exp\left(-\rho G\frac{y}{\cos\theta}\right). \tag{6}$$

The nonscattering transmission factor is thus given by

$$\tau_b'' = \frac{Q}{Q_o} = \exp\left(-K_b\rho y\right), \tag{7}$$

where $K_b = G/\cos\theta$ groups leaf orientation and zenith angle into a single parameter which is referred to as the blackbody attenuation coefficient because it describes the attenuation when the leaves are perfect radiation absorbers (black bodies). ρy gives the leaf area index of canopy above point y.

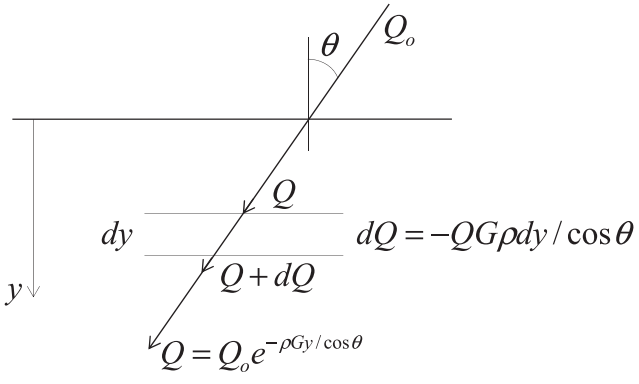

Figure 3. Illustration of radiation attenuation through a canopy that results in Beer's law.

3.1.2.2. Radiation Transmission With Scattering in an Infinitely Deep Canopy

[25] The attenuation in equation (7) does not consider scattering of light intercepted by the canopy. To account for scattering we use an approximation following *Monteith and Unsworth* [1990] that radiation from an incremental layer is scattered equally in an upward and downward direction and that scattering is along the same path as the incoming light. This approximation, strictly true only for leaves oriented perpendicular to the light beam, has been suggested and used as reasonable approximation for other angles to obtain analytic results [*Goudriaan*, 1977; *Monteith and Unsworth*, 1990] where otherwise radiation in multiple directions would need to be modeled. With this approximation streams of both downward and upward radiation need to be considered, hence the name two stream model, leading to

$$-dU = -UK_b\rho dy + UK_b\rho\frac{\alpha}{2}dy + QK_b\rho\frac{\alpha}{2}dy \tag{8}$$

$$dQ = -QK_b\rho dy + UK_b\rho\frac{\alpha}{2}dy + QK_b\rho\frac{\alpha}{2}dy. \tag{9}$$

In these equations α is the leaf scattering coefficient, Q and U (W m^{-2}), are intensity of the downward and upward beams, respectively (Figure 4). These equations account for the reduction in intensity of each beam due to interception, similar to Beer's law, but with scattering from each incremental layer assumed to be half upward and half downward. These equations are referred to as the Kubelka and Monk equations [*Monteith and Unsworth*, 1990]. Note that these are written for y positive in the downward direction.

[26] The pair of differential equations (8) and (9) have a general solution (see the Appendix)

$$Q(y) = \frac{1}{2}\left[C_1\left(1-\frac{1}{k'}\right)\exp\left(k'K_b\rho y\right) + C_2\left(1+\frac{1}{k'}\right)\exp\left(-k'K_b\rho y\right)\right] \tag{10}$$

$$U(y) = \frac{1}{2}\left[-C_1\left(\frac{1}{k'}+1\right)\exp\left(k'K_b\rho y\right) + C_2\left(\frac{1}{k'}-1\right)\exp\left(-k'K_b\rho y\right)\right], \tag{11}$$

where C_1 and C_2 (W m^{-2}) are integration constants and $k' = \sqrt{1-\alpha}$.

[27] For an infinitely deep canopy with $y = 0$ at the top of the canopy, a beam penetrating the canopy is reduced to

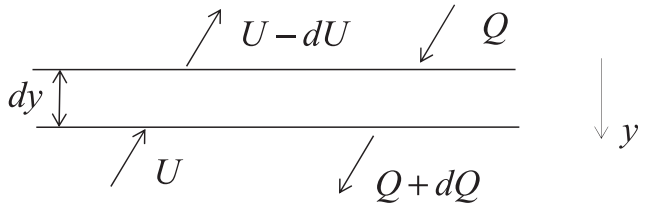

Figure 4. Incremental changes in upward and downward radiation beams calculated using equations (8) and (9).

*The term is correct here and throughout. The article as originally published appears online.

zero ($Q = 0$) when $y \to \infty$ (measured downward). This condition results in $C_1 = 0$. With this boundary condition, equations (10) and (11) reduce to

$$Q(y) = \frac{C_2}{2}\left(1 + \frac{1}{k'}\right)\exp\left(-k' K_b \rho y\right) \tag{12}$$

$$U(y) = \frac{C_2}{2}\left(\frac{1}{k'} - 1\right)\exp\left(-k' K_b \rho y\right). \tag{13}$$

These represent an exponential decrease in light intensity into the canopy similar to equation (7) but with the exponent reduced by a factor k'. k' quantifies the effect of multiple scattering on light penetration. The value of C_2 is related to the top boundary condition, Q_o. The deep canopy solution, equation (12), yields the deep canopy multiple scattering transmission factor

$$\tau_b' = \frac{Q(y)}{Q_o} = \exp\left(-k' K_b \rho y\right). \tag{14}$$

This is a modification to Beer's law for radiation transmission of a single beam accounting for scattering.

[28] The upward reflection factor giving the fraction of radiation reflected back from a deep canopy with multiple scattering, β' can be estimated using equations (12) and (13) as

$$\beta' = \frac{U(y)}{Q(y)} = \frac{1 - k'}{1 + k'}. \tag{15}$$

[29] The above is for a single beam. For diffuse radiation the approach is to recognize that it is composed of single beam components from each direction $Q(\theta)$. The component of each of these normal to the surface is integrated over the hemisphere. With this approach diffuse radiation above and in the canopy is given by $\int_\Omega Q(\theta)\cos\theta d\Omega$ and $\int_\Omega Q(\theta)\tau_b'\cos\theta d\Omega$, respectively. In this integral τ_b' depends on K_b which is function of θ. Using these integrals, the transmission factor for diffuse radiation, τ_d' may be expressed as

$$\tau_d' = \frac{\int_\Omega Q(\theta)\tau_b'\cos\theta d\Omega}{\int_\Omega Q(\theta)\cos\theta d\Omega}, \tag{16}$$

where $Q(\theta)$ is the radiance of the sky from the direction θ, $d\Omega = \sin\theta d\theta d\phi$ is the solid angle for integration over the hemisphere, θ is the zenith angle in the range $(0, \pi/2)$ and ϕ is the azimuth angle in the range $(0, 2\pi)$.

[30] Assuming that radiation in the canopy is isotropic, $Q(\theta) = Q$, a constant; the solution to this equation [*Nijssen and Lettenmaier*, 1999] is

$$\tau_d' = \left[(1 - k' G\rho y)\exp\left(-k' G\rho y\right) + (k' G\rho y)^2 E_i(1, k' G\rho y)\right], \tag{17}$$

where $E_i(n,x)$ with n a nonnegative integer is the exponential integral, defined as

$$E_i(n,x) = 2\int_1^\infty \frac{\exp(-xt)}{t^n} dt. \tag{18}$$

Because diffuse radiation is just an integral of direct beam components over the hemisphere, the upward diffuse radiation reflection factor for a deep canopy is also given by equation (15).

3.1.2.3. Radiation Transmission With Scattering in a Finite Canopy

[31] The radiation transmission factors shown in equations (14) and (15) above are for an infinitely deep canopy. We obtain the solution for a finite canopy by recursive superposition of the deep canopy solution (Figure 5). At depth y into a deep canopy, the solution is

$$Q_1(y) = Q_o \tau'(y) \tag{19}$$

$$U_1(y) = \beta' Q_o \tau'(y), \tag{20}$$

where $\tau'(y)$ may be τ_b' from equation (14) or τ_d' from equation (17).

[32] Now suppose the canopy has a finite depth, D (m), and incident radiation, Q_o, at the top with no incident radiation from below the base. At the base, $y = D$, the upward radiation U should be zero rather than $U_1(D)$ given by equation (20). This can be obtained by adding (superposing) a solution for radiation input $-U_1(D)$ at the base.

[33] Applying equations (14) and (15) but for $-U_1(D)$ incident from below, we get

$$U_2(y) = -U_1(D)\tau'(D - y) = -\beta' Q_o \tau'(D)\tau'(D - y) \tag{21}$$

$$Q_2(y) = -\beta' U_1(D)\tau'(D - y) = -(\beta')^2 Q_o \tau'(D)\tau'(D - y). \tag{22}$$

This would result in $Q_2(0) = -\beta' U_1(D)\tau'(D) = -(\beta')^2 Q_o \cdot (\tau'(D))^2$ at the top where $y = 0$. As before the top boundary condition $Q_2(0)$ should be zero. This necessitates superposing another solution using incident radiation input of $-Q_2(0)$ at the top, which gives

$$Q_3(y) = -Q_2(0)\tau'(y) = (\beta')^2 Q_o (\tau'(D))^2 \tau'(y) \tag{23}$$

$$U_3(y) = -\beta' Q_2(0)\tau'(y) = (\beta')^3 Q_o (\tau'(D))^2 \tau'(y). \tag{24}$$

Continuing this process recursively, the finite depth solution is

$$Q(y) = Q_1(y) + Q_2(y) + Q_3(y) + \ldots \tag{25}$$

$$U(y) = U_1(y) + U_2(y) + U_3(y) + \ldots \tag{26}$$

These infinite series can be evaluated to give

$$Q(y) = Q_o \frac{[\tau'(y) - (\beta')^2 \tau'(D)\tau'(D - y)]}{1 - (\beta')^2 (\tau'(D))^2} \tag{27}$$

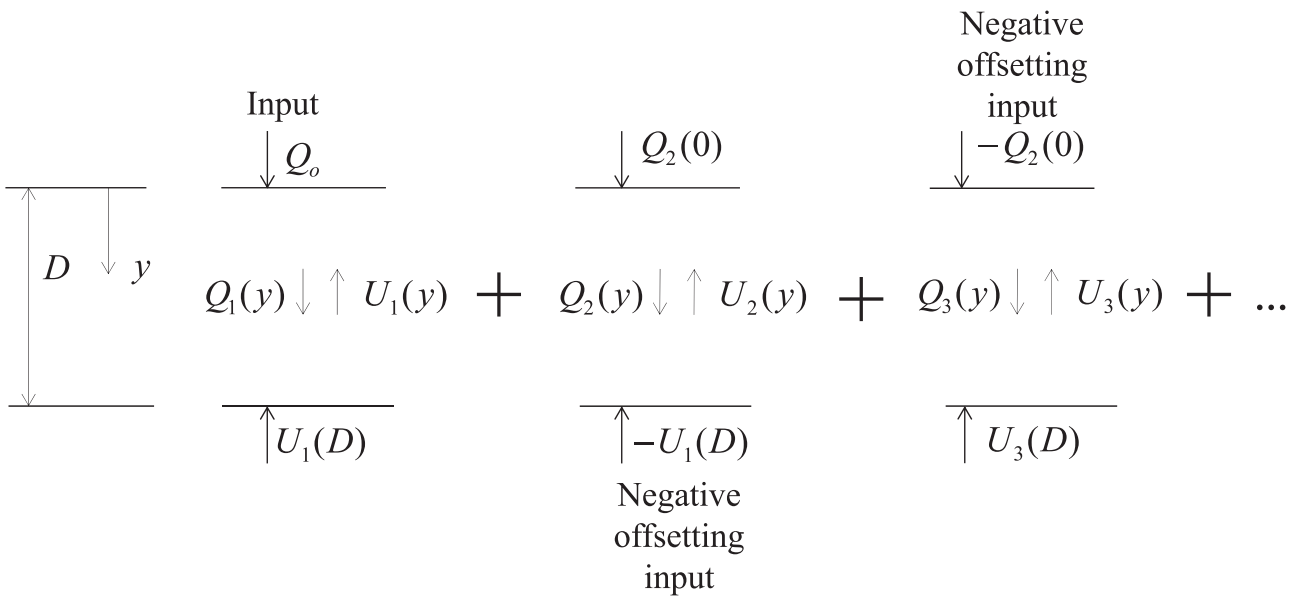

Figure 5. Sequence of superposed deep canopy solutions that offset the deep canopy backscatter by adding another deep canopy solution in the opposite direction with negative input to obtain finite canopy solution.

This should be beta single prime

$$U(y) = Q_o \frac{[\beta\tau'(y) - (\beta')\tau'(D)\tau'(D-y)]}{1-(\beta')^2(\tau'(D))^2}. \quad (28)^*$$

Using equations (27) and (28), the finite canopy transmission and reflection factors, τ and β can be calculated as

$$\tau = \frac{Q(D)}{Q_o} = \frac{\tau'(D)[1-(\beta')^2]}{1-(\beta')^2(\tau'(D))^2} \quad (29)$$

$$\beta = \frac{U(0)}{Q_o} = \frac{\beta'[1-(\tau'(D))^2]}{1-(\beta')^2(\tau'(D))^2}. \quad (30)$$

Equations (29) and (30) can be used for both direct and diffuse radiation. The fraction of direct radiation transmitted through the canopy, τ_b, and diffuse radiation transmitted through the canopy, τ_d, can be calculated using $\tau' = \tau_b'$ and $\tau' = \tau_d'$, respectively, in equation (29). Similarly the direct and diffuse fractions of radiation reflected back from the canopy in an upward direction, β_b and β_d can be calculated using $\tau' = \tau_b'$ and $\tau' = \tau_d'$, respectively, in equation (30).

[34] In evaluating (29) and (30) in the direct radiation case, using equation (14)

$$\tau_b'(D) = \frac{Q(D)}{Q_o} = \exp(-k' K_b \rho D) = \exp\left(-k' \frac{G}{\cos\theta} LF\right). \quad (31)$$

Here ρD, the leaf area index over the full canopy depth D has been replaced by LF where L is the tree level leaf area index and F is the canopy cover fraction accounting for the fact that trees may not completely cover the domain. The product LF is effectively a canopy level leaf area index. We assume a constant leaf orientation factor, $G = 0.5$, representing isotropic leaf orientations.

[35] In the diffuse radiation case, using equation (17)

$$\tau_d'(D) = [(1-k'G\rho D)\exp(-k'G\rho D) + (k'G\rho D)^2 E_i(1, k'G\rho D)] = [(1-k'GLF)\exp(-k'GLF) + (k'GLF)^2 E_i(1, k'GLF)] \quad (32)$$

We treat G, L, and F as constants, neglecting any effects canopy intercepted snow may have on canopy radiation transmission and reflectance.

[36] Figure 6 compares the transmittance of direct and diffuse solar radiation calculated using the two stream approach (equation (29)) with the transmittance of radiation calculated using Beer's law (equation (7)) as a function of zenith angle. A significant increase in transmittance over

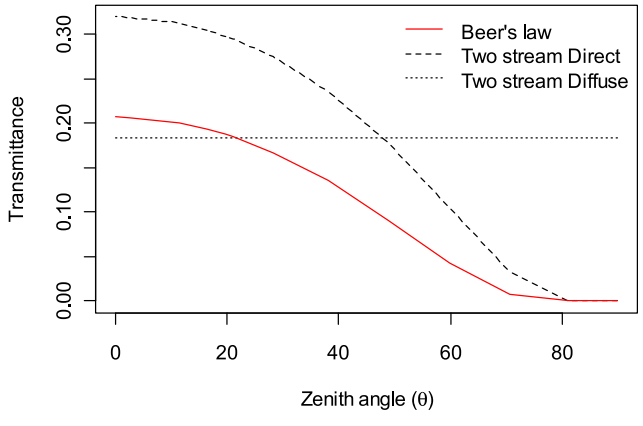

Figure 6. Radiation transmittance as a function of solar zenith angle calculated using Beer's law (equation (7)) and the two stream approach (equation (29)) developed in this work for canopy level leaf area index (LF) of 3.15 and leaf scattering coefficient α of 0.5.

*The equation is correct here. The article as originally published appears online.

the Beer's law attenuation occurs due to multiple scattering in the canopy.

3.2. Longwave Radiation

[37] Longwave radiation originates from three possible sources: the sky, snow surface and the canopy. Longwave radiation from each of these sources is considered to be diffuse radiation that penetrates through or is scattered by the canopy according to diffuse radiation transmission processes. However the scattering of longwave radiation is much less than that of shortwave radiation because the leaf-scale reflectance for longwave, $\alpha = 1 - \varepsilon_c$, is very close to 0, where ε_c is canopy emissivity. Longwave radiation emitted by the canopy, Q_{lc}, is calculated as $\varepsilon_c \sigma {T_c}^4 (1 - \tau_d)$, where σ is the Stefan–Boltzmann constant (5.67×10^{-8} W m^{-2} K^{-4}), T_c (K) is the canopy temperature and $(1 - \tau_d)$ accounts for the fraction of the canopy exposed. The longwave radiation emitted from the atmosphere, Q_{li}, and snow surface, Q_{le}, are calculated as $\varepsilon_a \sigma {T_a}^4$ and $\varepsilon_s \sigma {T_s}^4$, where ε_a and ε_s are air and snow emissivity, and T_a (K) and T_s (K) are air and snow surface temperatures, respectively.

[38] We use Satterlund's parameterization [*Satterlund*, 1979] of air emissivity for clear sky conditions

$$\varepsilon_{acls} = 1.08\left[1 - \exp\left(-\left(\frac{e_a}{100}\right)^{T_a/2016}\right)\right], \tag{33}$$

where e_a is air vapor pressure (Pa). To adjust for cloud cover we use

$$\varepsilon_a = C_f + (1 - C_f)\varepsilon_{acls}, \tag{34}$$

where C_f is the cloud cover fraction.

3.3. Multiple Reflections Between the Canopy and Surface

[39] The above canopy transmission parameterization represents multiple scattering within the canopy. There is however the opportunity for light to reflect multiple times between the canopy and surface. Section 3.3 describes how these multiple reflections are numerically evaluated.

[40] For solar radiation we treat the canopy as a single layer with internal multiple scattering accounted for as described above. When each component of the solar beam (direct and diffuse) impacts the canopy; part of it is absorbed, part is reflected and part is transmitted. The reflected part is lost upward. The transmitted part is absorbed or reflected at the surface; and the part reflected from the surface is again absorbed, transmitted or reflected by the canopy leading to multiple reflections between the canopy and surface. These multiple reflections are assumed to be diffuse and the reflection by or transmission through the canopy is calculated using τ and β from equations (29) and (30). Radiation that is reflected from the surface is calculated using snow surface albedo, A, which is modeled based on snow surface age and depth [*Tarboton and Luce*, 1996; *Tarboton et al.*, 1995]. The effects of forest litter on the beneath canopy snow albedo are not modeled.

[41] After multiple reflections the overall fractions of solar radiation from above transmitted and reflected by the canopy, f_1 and f_3 (Figure 7) are given by

$$f_1 = \frac{(1 - A)\tau}{1 - A\beta_d(1 - \tau_d)} \tag{35}$$

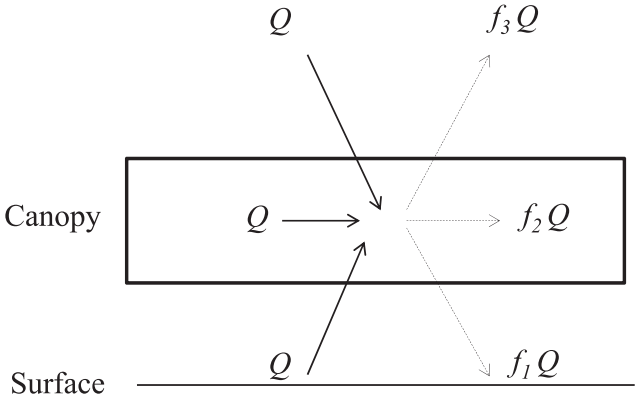

Figure 7. Factors to quantify the ultimate partitioning of any radiative input Q into components absorbed by the surface, f_1, or canopy, f_2, or lost to the sky above, f_3. Q may represent solar or longwave radiation from the sky/atmosphere, canopy or surface. $f_1 + f_2 + f_3 = 1$.

$$f_3 = \frac{(1 - A)\beta + A\tau\tau_d}{1 - A\beta_d(1 - \tau_d)}. \tag{36}$$

Here τ and β are direct or diffuse factors depending on whether the incident radiation is direct or diffuse. The fraction of radiation intercepted by the canopy, f_2 can be calculated by subtracting (35) and (36) from 1. Summing up fractions from both direct and diffuse beams yields

$$Q_{sns} = f_{1b}Q_b + f_{1d}Q_d, \tag{37}$$

$$Q_{cns} = f_{2b}Q_b + f_{2d}Q_d, \tag{38}$$

$$Q_{rns} = f_{3b}Q_b + f_{3d}Q_d, \tag{39}$$

where Q_{sns}, Q_{cns}, and Q_{rns} are subcanopy net solar radiation, canopy net solar radiation and reflected solar radiation lost upward, respectively. Here subscripts b and d in f_1, f_2, and f_3 refer to direct and diffuse solar radiation, respectively.

[42] For longwave radiation we ignore multiple reflections as both plants and snow strongly absorb longwave radiation (absorptivity equal to emissivity close to 1). Like shortwave radiation, longwave radiation from all three sources is partitioned into fractions: f_1 (absorbed at surface), f_2 (absorbed in canopy) and f_3 (lost to sky). Summing up fractions from all sources yields

$$Q_{\mathrm{snl}} = f_{1i}Q_{li} - Q_{le} + f_{1e}Q_{le} + f_{1c}Q_{lc}, \tag{40}$$

$$Q_{\mathrm{cnl}} = f_{2i}Q_{li} + f_{2e}Q_{le} + f_{2c}Q_{lc} - 2Q_{lc}, \tag{41}$$

$$Q_{\mathrm{rnl}} = f_{3i}Q_{li} + f_{3e}Q_{le} + f_{3c}Q_{lc} + Q_{lc}, \tag{42}$$

where Q_{snl}, Q_{cnl}, and Q_{rnl} are subcanopy net longwave radiation, canopy net longwave radiation and reflected net longwave radiation lost upward, respectively. The subscripts i, e, and c in f_1, f_2, and f_3 are used to represent the

radiation from sky, snow surface and from the canopy, respectively. The fractions f_1, f_2, and f_3 for longwave radiation are calculated as

$$f_{1i} = \varepsilon_s \tau_d, f_{2i} = (1-\tau_d)\varepsilon_c + \tau_d(1-\varepsilon_s), f_{3i} = (1-\tau_d)(1-\varepsilon_c),$$
$$f_{3e} = \tau_d, f_{2e} = (1-\tau_d)\varepsilon_c, f_{1e} = (1-\tau_d)(1-\varepsilon_c),$$
$$f_{1c} = \varepsilon_s, f_{3c} = \tau_d(1-\varepsilon_s) \text{ and } f_{2c} = (1-\tau_d)(1-\varepsilon_s)\varepsilon_c. \quad (43)$$

With emissivities close to 1 there is a very small error in these equations that we neglect due to the neglect of multiple reflections. The net longwave and shortwave radiation calculated here are used with other energy fluxes in the snowmelt model energy balance equations to provide the net energy that drives the snowmelt in the open, beneath the canopy or within the canopy.

4. Model Application and Simulation Results

[43] Simulations were performed for the period of January 2008 to July 2008, December 2008 to July 2009 and January 2009 to July 2010 to estimate the radiation and snowmelt in the open and within and below the deciduous and coniferous forest using the hourly meteorological inputs of precipitation, temperature, wind speed and relative humidity. For forested areas, the open site meteorological variables are assumed representative of conditions at a height of 2 m above the forest canopy. Wind speeds within and beneath the canopy were calculated working downward from above the canopy using exponential and logarithmic wind profiles [*Bonan*, 1991; *Koivusalo*, 2002]. Input precipitation data were taken from the SNOTEL site located in a small opening in the conifer forest and the other meteorological input data were obtained from the shrubs B (SB) open site (Figure 1). Leaf area index values for conifer and deciduous forest were chosen based on the ranges of values that are found in the literature, but with adjustments within these ranges to fit our data. Canopy coverage fraction was estimated based on our field observations of the canopy, but not on formal measurements. Thermal conductivity of snow and soil were adjusted (calibrated) to obtain a better match between modeled and observed surface temperature at the central open site for the whole simulation period. This adjustment was needed to correctly estimate the energy fluxes, including longwave radiation that is based on surface temperature. The thermal conductivity parameters obtained from calibration at the open site were used in both open and forest settings. By calibrating thermal conductivity at the open site we separate the calibration issue from the evaluation of the canopy radiation model that is the main focus of this paper. Other parameters follow the original UEB model [*Tarboton and Luce*, 1996; *You*, 2004] are presented in Table 2.

[44] The model is able to predict the SWE, snow surface temperature, snow average temperature, canopy wind speed, radiation, energy fluxes and interception for both open and forest areas. Measurements of the four radiation components and surface temperature were available for the years 2009 and 2010, but not 2008 at the open site. We compare measured and modeled radiation components for 2009 and 2010 to validate the models calculation of open (above canopy) radiation. We then drive the model by inputs of measured open incoming shortwave and longwave radiation for 2009 and 2010, and modeled incoming shortwave and longwave radiation in 2008. 2008 serves as a check of the more complete model including atmospheric radiation parts. We evaluate the modeling of canopy radiation transmission processes by comparing modeled and observed below canopy net radiation and SWE. The SWE comparisons serve as an aggregate test of all aspects of the model, not limited to correct radiation transmission.

4.1. Four Radiation Components and Surface Temperature

[45] The four radiation components were continuously measured at the central tower site for two winters (2008–2009 and 2009–2010). Measurements were compared with

Table 2. Model Parameters

Name	Values	Basis
Air temperature above which precipitation is all rain (T_r)	3°C	*Tarboton et al.* [1995], *U.S. Army Corps of Engineers* [1956]
Air temperature below which precipitation is all snow(T_{sn})	−1°C	*Tarboton et al.* [1995], *U.S. Army Corps of Engineers*, [1956]
Emissivity of snow (ε_s)	0.98	*Tarboton et al.* [1995]
Ground heat capacity (C_g)	2.09 kJ kg^{-1} C^{-1}	*Tarboton et al.* [1995]
Nominal measurement of height for air temperature and humidity (Z)	2.0 m	*Tarboton et al.* [1995]
Surface aerodynamic roughness (Z_o)	0.01 m	*You* [2004]
Soil density (ρ_g)	1700 kg m^{-3}	*Tarboton et al.* [1995]
Liquid holding capacity of snow (L_c)	0.05	*Tarboton et al.* [1995]
Snow saturated hydraulic conductivity (K_s)	20 m h^{-1}	*Tarboton et al.* [1995]
Visual new snow albedo (α_{vo})	0.85	*Tarboton et al.* [1995]
Near IR new snow albedo (α_{iro})	0.65	*Tarboton et al.* [1995]
Bare ground albedo (α_{bg})	0.25	*Tarboton et al.* [1995]
Thermally active depth of soil (d_e)	0.1 m	*You* [2004]
Thermal conductivity of snow (λ_s)	3.6 Wm^{-1} K^{-1}	Adjusted
Thermal conductivity of soil (λ_g)	14.4 Wm^{-1} K^{-1}	Adjusted
Atmospheric transmittivity for cloudy conditions (a_s)	0.25	*Shuttleworth* [1993]
Atmospheric transmittivity for clear conditions ($a_s + b_s$)	0.75	*Shuttleworth* [1993]
Ratio of direct to total radiation for clear sky (λ)	6/7	Calculated
Richardson number upper bound for stability correction (Ri_{max})	0.16	*Koivusalo* [2002]
Leaf scattering coefficient (conifer/deciduous) (α)	0.5	*Norman* [1979]
Emissivity of canopy (conifer/deciduous) (ε_c)	0.98	*Bonan* [1991]
Interception unloading rate (U_s)	0.00346 h^{-1}*	*Hedstrom and Pomeroy* [1998]

Thermal conductivity of snow should be 0.278 W m^{-1} K^{-1}

Thermal conductivity of soil should be 1.11 W m^{-1} K^{-1}

*The value is correct here. The article as originally published appears online.

model outputs aggregated to a daily time scale so as to mask the effect of diurnal fluctuations and to better see daily total comparisons (Figure 8). Simulated values of solar radiation (incoming and reflected) and longwave radiation (incoming and outgoing) compared well with the observations for the 2 years with measured radiation data (2009 and 2010). The modeled incoming radiation that tracks observations reasonably well confirms cloud cover and atmospheric transmittivity parameterizations based on diurnal temperature range. The modeled outgoing radiation that tracks observation reasonably well serves to check the model albedo and surface temperature and emissivity representations. The high correlation and modest BIAS and RMSE values in scatterplots (Figure 8), relative to the ranges of these measurements also confirm the model effectiveness. Some of the differences may also be due to measurement errors such as the sensor sometimes having snow on it in this winter environment.

[46] The outgoing longwave radiation, and many other fluxes at the snow surface, are functions of the snow surface temperature, which itself results from the balance of energy fluxes to and from the surface. This is why the representation of surface temperature by a snowmelt model is important. The model predictions of surface temperature at the open (snow/shrub) central tower site compared reasonably well to measured values (Figure 9). Some zero values seen in the model differed from observed values (Figure 9) because of the model retaining snow a few days longer than was observed. Temperature values above 0°C occur on days without snow.

4.2. Net Radiation

[47] The model simulation of below canopy net radiation was compared with the net radiation measured below conifer (CA) forest and deciduous (DB) forest canopy, aggregated to daily time scale (Figure 10). The model predictions of net radiation followed the below canopy net radiation measurements reasonably well with correlation of about 0.90 for both forest types (Figure 10). Also, small BIAS and RMSE values were observed. In Figure 10 the scatterplots for 2008 where inputs were modeled radiation are separated from scatterplots for 2009 and 2010 where inputs are measured longwave and shortwave radiation from the open site. Both the time series and scatterplots for 2008 showed that the predictions of below canopy net radiation from the modeled above canopy radiation were not significantly different than those predicted using the measured above canopy radiation as input. For all these results the

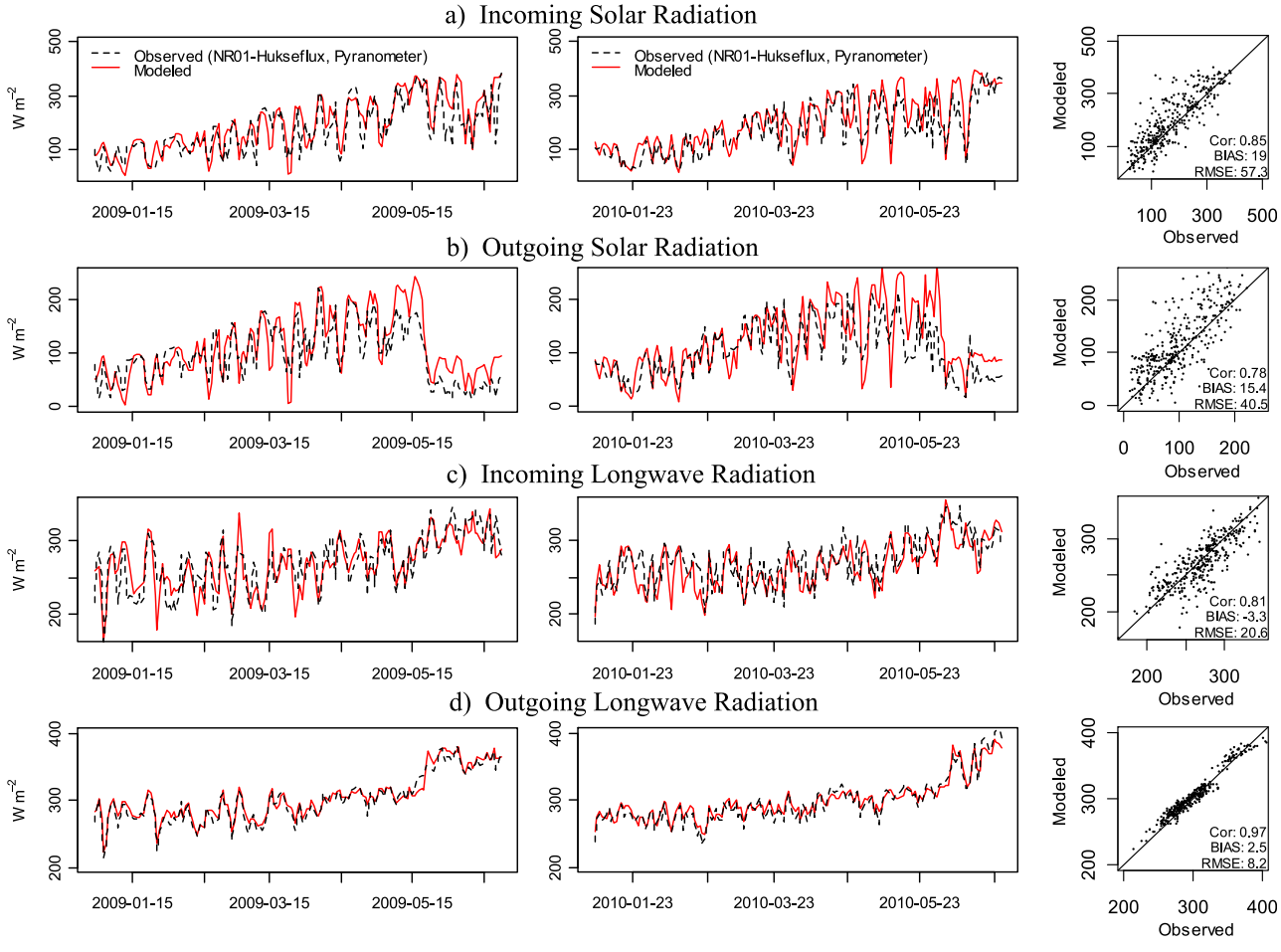

Figure 8. Time series and scatterplots of observed and modeled mean daily radiation components: (a) incoming solar radiation, (b) outgoing (reflected) solar radiation, (c) incoming longwave radiation, (d) outgoing longwave radiation.

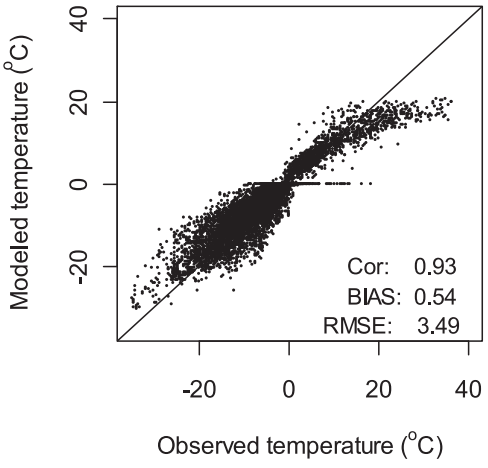

Figure 9. Scatterplot of observed and modeled hourly surface temperature for the year 2008 and 2009 at central tower (snow/shrub).

modeled net radiation tended to have a slight overprediction bias compared to the measurements in the early period. However the model showed relatively good agreement with observations during spring, which is important for calculating melt. The BIAS and RMSE values were found to be slightly higher for deciduous forest in comparison to conifer forest.

[48] To further evaluate the model, modeled beneath canopy daily net radiation versus open area daily net radiation was compared to observations of the same quantities each year for both conifer and deciduous forest (Figure 11). The solid lines in the Figure are linear least square fits constrained to go through the origin: red for simulated and black for the measured values, with the slopes given in the plots. These graphs show what fraction of open net radiation is measured beneath the canopy and how the model is able to represent this for both coniferous and deciduous forest. These figures indicate a slight over prediction bias in the model.

[49] The original UEB model uses linear relationships to reduce shortwave, longwave or net radiation beneath the canopy based on forest cover fraction, F. Wind speed and the corresponding heat and vapor fluxes are reduced by factor (1–0.8 F). Table 3 compares the new model simulated radiation with old model results. The old model predictions of beneath canopy radiation, especially the longwave radiation is very low. The old model reduces the incoming longwave radiation beneath the canopy, however the beneath canopy longwave radiation increases because of the higher emissivity of the canopy in comparison to the atmosphere.

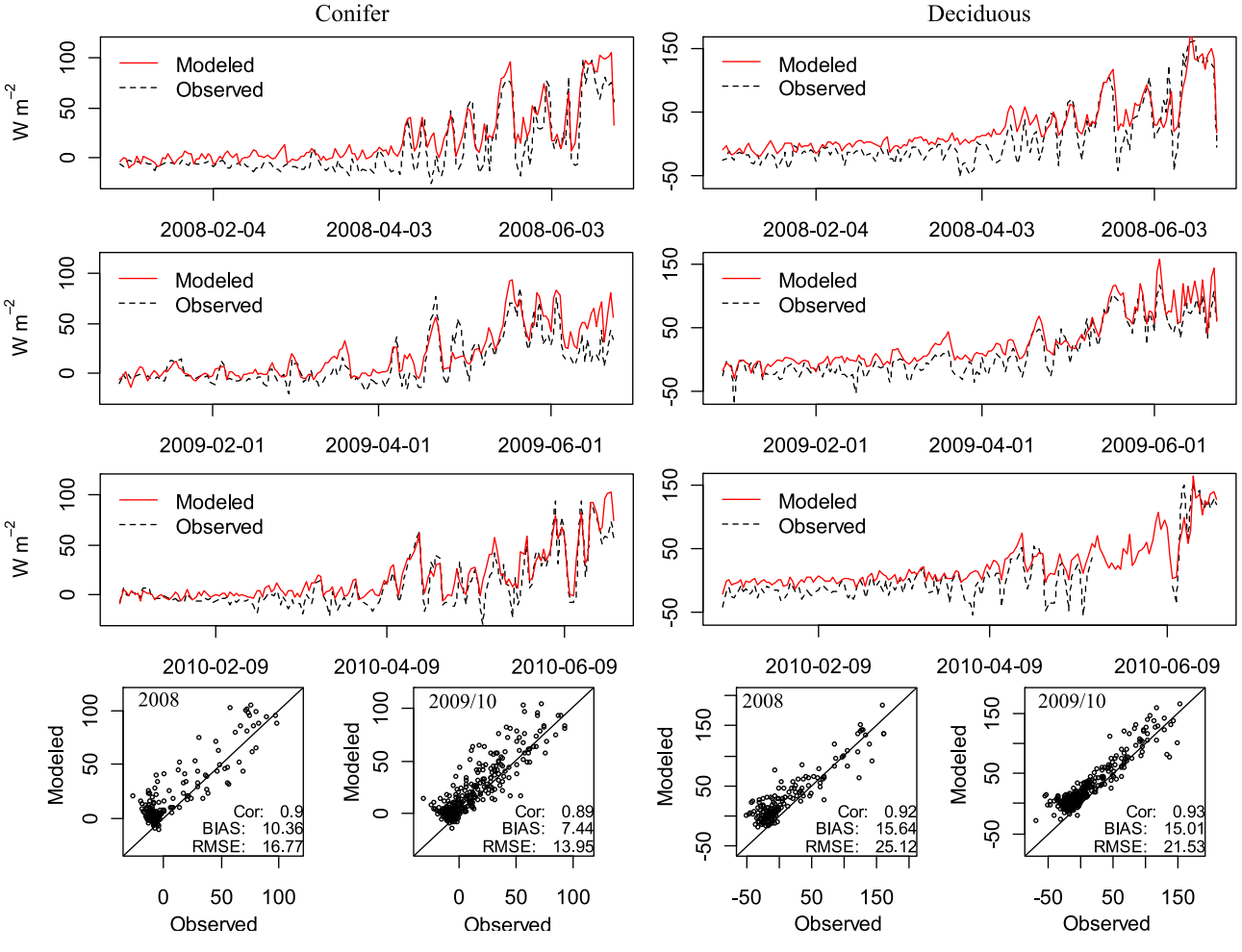

Figure 10. Time series and scatterplots of mean daily net radiation: observed and modeled beneath the deciduous and coniferous forest canopy.

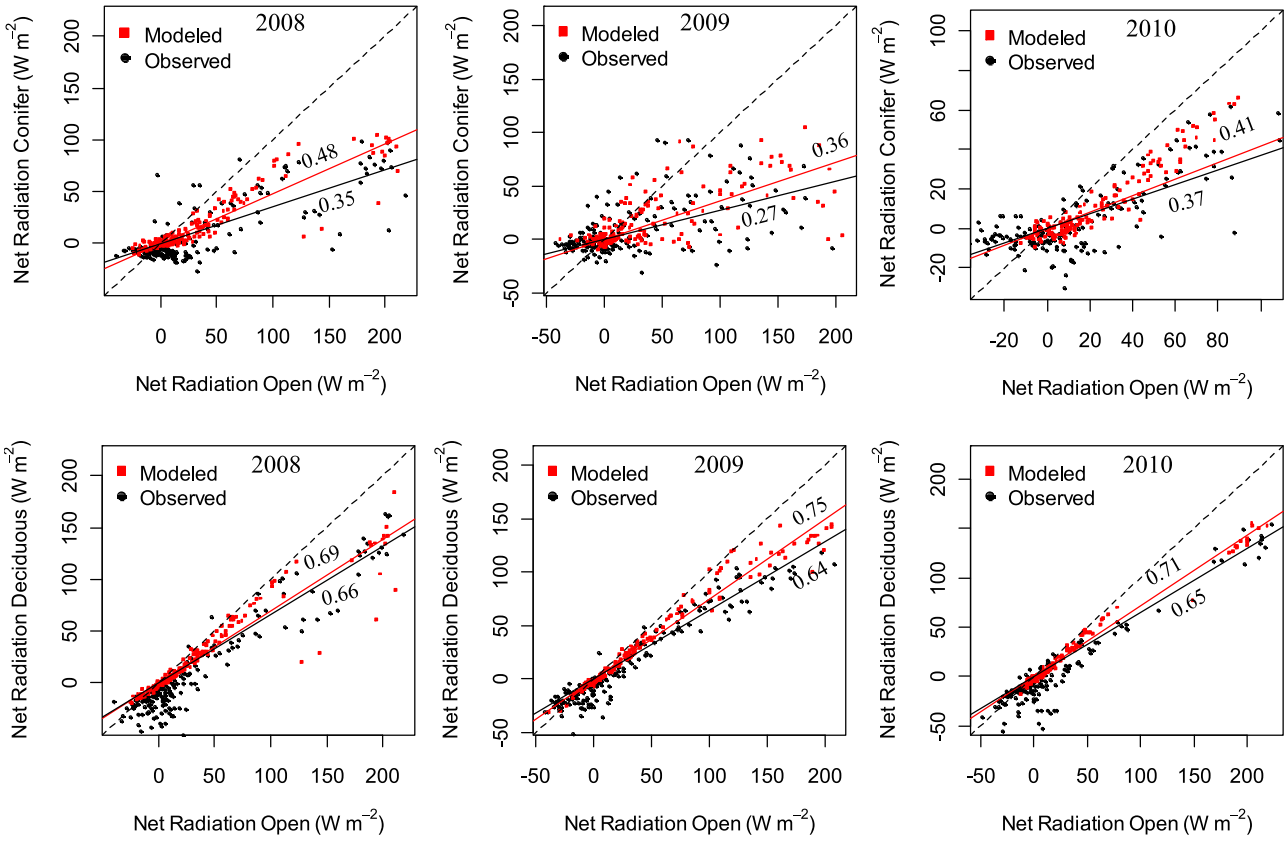

Figure 11. Observed and modeled below canopy net radiation presented in comparison to open area net radiation (observed and modeled) for the years 2008, 2009 and 2010. Solid lines are least square fits constrained to go through the origin. The regression slope is indicated for each line and gives the average fraction of under canopy net radiation as compared to net radiation in the open.

Also, while calculating beneath canopy radiation, the original model does not consider leaf area index and provides similar solutions for two different forest types with different leaf area with same canopy cover fraction.

4.3. Snow Water Equivalent

[50] Snow depths were monitored in the field by manually probing depth at twenty one locations and automatically with snow depth sensors mounted in on twelve weather station towers (Figure 1). These depths were used with density sampled over the depth of two snow pits to derive snow water equivalent, SWE (m), in each of the vegetation classes. The model was initialized with measured SWE values (from snow depth sensors) on 1 April and run for the period between 1 April to 30 June to simulate the SWE values that were compared with observations made in the open, and beneath the deciduous and coniferous canopies (Figure 12). The simulation period was chosen to cover the melt period only, because the canopy radiation transmission is dominant in driving snowmelt, while other processes like interception and sublimation are more important earlier in the snow season. The observed SWE values (from depth sensors) below the conifer and deciduous forest are averages of the measurements in each forest type. The observed SWE for the open area is taken from a single site (SB) chosen because this site was least affected by wind drift and scouring. All the meteorological input variables used in this work were taken from the SB site. Field

Table 3. Comparison of New and Original UEB Model Radiation Components With Some Measurements

Mean Energy Fluxes (W m^{-2}) Averaged for 1 April to 30 June Melt Period 2009 and 2010		Open, Measured	Deciduous			Conifer		
			Measured	New UEB	Old UEB	Measured	New UEB	Old UEB
Surface/subcanopy solar radiation	$Q_{ss}\downarrow$	231.1	–	147.1	66.7	–	49.2	68.2
	$Q_{ss}\uparrow$	–	–	82.3	44.7	–	32.5	45.7
Surface/subcanopy longwave radiation	$Q_{sl}\downarrow$	284.2	–	306.2	85.0	–	325.5	85.1
	$Q_{sl}\uparrow$	–	–	315.9	92.6	–	310.1	92.7
Surface/subcanopy net solar radiation	$Q_{sns}\downarrow$	–	–	64.8	22.0	–	16.8	22.5
Surface/subcanopy net longwave radiation	$Q_{snl}\downarrow$	–	–	−9.7	−7.6	–	15.4	−7.6
Surface/subcanopy net radiation	$Q_{sn}\downarrow$	70.3	39.3	55.1	14.4	22.9	32.2	14.9

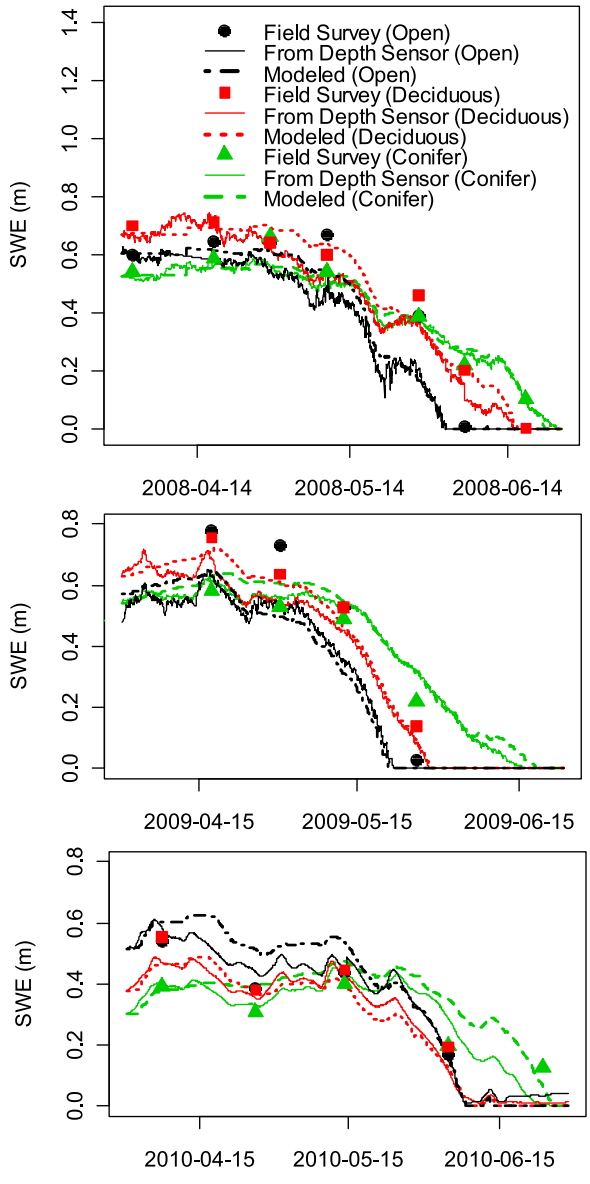

Figure 12. Snow Water Equivalent (SWE) comparison across different vegetation classes for the 2008, 2009 and 2010 snowmelt periods.

surveyed SWE values were quite variable. The field surveyed SWE values for each vegetation class presented here are from locations selected to have their first SWE value most closely matching the SWE value for that vegetation class calculated from snow depth sensors and used to initialize the model. The snow melt and SWE values in the open area and beneath the deciduous and conifer forest canopy were reasonably predicted by the model.

5. Discussion

[51] The radiation transmission model we developed is based on a simple two stream approximation that uses leaf area index as a key parameter and provides solution similar to Beer's law but adjusted for multiple scattering. The model is not intended to replace detailed multilayer radiation transfer models that consider the leaf orientation, inclination and distribution for each layer separately, but is suggested as a parsimonious approach when detailed information for each canopy layer is not available.

[52] Overall, in examining the results, we see that the model simulated radiation values were in general agreement with the observed radiation values below different forest canopies. We found that there was a tendency to over predict early season net radiation (Figure 10) and overall slightly over predict the fraction of open net radiation found beneath a canopy (Figure 11). These effects were generally small and may be due to many factors. The radiation transmission model has a number of simplifications and does not represent canopy architecture, leaf orientation and layering effects. The model calculates average radiation beneath the canopy ignoring vertical and horizontal forest heterogeneity that result in spatial variability of radiation beneath the canopy. Also, the radiation sensor may not have been ideally placed to measure average radiation.

[53] There are also uncertainties associated with the leaf level reflectances that were taken from the literature and estimates of leaf area index. There might also be measurement errors. During the early winter the upper part of the net radiometer had a tendency to catch snow which may result in bias in the measurements. There could also be uncertainty in the partitioning of incoming solar radiation. As direct and diffuse radiation attenuates differently in the canopy, the uncertainty in partitioning may also lead to errors in canopy radiation transmission processes. Small errors in predicting the canopy or surface temperature may cause errors in representing the longwave radiation that has a large contribution to net radiation. Also, the albedo of snow beneath the forest canopy is influenced by the forest litter.

[54] The radiation transfer processes in the conifer canopy was better represented by the model in comparison to that in deciduous canopy (Figure 10). The problem in the deciduous site could be the poor representation of canopy structure. In our simulation we assumed similar leaf structures and reflectivity for both deciduous and conifer trees. However the emissivity and scattering characteristics of these two species can be different, as one is leaved and the other is leafless tree during the winter.

[55] Given all the uncertainties and assumptions in the model, the model seems to be successful in terms of predicting the net radiation for snowmelt (Figure 10). The model's generally good prediction of net radiation is reflected in SWE and snowmelt comparisons for open, beneath deciduous and conifer forest canopies (Figure 12). Slower ablation as forest density increases (open to deciduous to conifer) is evident in the observations. This effect is evident in the model results, reflecting the model's capability to, in aggregate, represent the processes driving snow melt in open and forested areas, with appropriate sensitivity to forest type.

[56] In the SWE comparisons using the full new UEB model, there are model changes in terms of the representation of other canopy processes such as snow interception/sublimation and turbulent fluxes of sensible heat and latent heat that have not been fully described or evaluated in this paper and that do, to some extent impact the results in Figure 12, and even to some extent the net radiation comparisons since they impact surface temperature. It is

simply not possible to isolate and evaluate only one set of processes in a system such as snow under a canopy where there are many interacting processes. Our focus on the melt period where radiation dominates the beneath canopy latent heat and sensible heat fluxes which totaled about 2% of beneath canopy net radiation serves as the best possible validation of the new radiation components added. Future work will more comprehensively evaluate the other new model components.

[57] The two stream multiscattering approach used here enables the quantification of the energy balance of the snowpack and simulation of snowmelt in forested environments without requiring detailed canopy structure inputs. The approach is simple enough to be applied in a spatially distributed way so as to explicitly represent variability in canopy processes in the simulation of snowmelt over a watershed in a relatively physically based fashion. This would take advantage of detailed spatial information such as different grid values of slope and aspect (to account for topography) and leaf area index and canopy coverage to quantify the vegetation. Advancing capability for remote sensing of these quantities [e.g., *Fassnacht et al.*, 1997; *Running et al.*, 1989; *Zheng and Moskal*, 2009] would benefit this modeling approach.

[58] While we have not quantitatively compared this approach to other approaches that require similar input information, we feel that the physically based rigor of the two-path multiscattering approach gives it a theoretical advantage that has been shown to, at least for our data, do a reasonable job of capturing sensitivity to canopy variability. Our model does not address transition effects such as solar radiation penetration to snow beneath a forest canopy near an opening, or shading of open areas by nearby forests. Further study to understand and quantify the impacts and importance of transitions on snow accumulation and melt is warranted.

6. Conclusions

[59] We developed a simple canopy radiation transfer model that looks similar to Beer's law but considers the multiple scattering and reflection of radiation in the canopy based on two radiation streams, upward and downward. The model estimates the radiation beneath the canopy, which is important to predict the snowmelt responsible for water supply, using leaf area index as the key canopy parameter. The model results agreed well with observed net radiation and SWE values beneath coniferous and deciduous forest canopies. The model had a weakness in predicting the radiation beneath the canopy during the early winter; however the prediction of radiation for the late winter and spring period was better. The model was able to capture the differences in ablation between open and forested areas and in coniferous and deciduous forest.

[60] The approach used here offers improvements over existing models that use simple linear reduction or Beer's law to attenuate radiation in a forest canopy. The canopy radiation transmission model developed in this work is an advance over Beer's law which does not account for multiple scattering of radiation. It uses a physically based approach to model absorption and scattering of radiation by the canopy, but limiting inputs to parameters that may be relatively easily obtained in the field or by remote sensing. Many of the canopy radiation transmission models used in snow modeling are either oversimplified and less physically relevant or over parameterized and require extensive inputs that are hard to obtain. The solution for multiple scattering in a canopy with finite depth using the two stream approximation given here is, to our knowledge, new. The findings from this work may be of interest not only to people who want to use the improved UEB model but also to the wider snow modeling community who want to better predict the beneath canopy radiation and energy balance with a parsimonious parameterization of the penetration of radiation through canopy in a forested environment.

Appendix: Solution to Equations (8) and (9)

[61] Equations (8) and (9) are

$$-dU = -UK_b\rho dy + UK_b\rho\frac{\alpha}{2}dy + QK_b\rho\frac{\alpha}{2}dy \tag{A1}$$

$$dQ = -QK_b\rho dy + UK_b\rho\frac{\alpha}{2}dy + QK_b\rho\frac{\alpha}{2}dy. \tag{A2}$$

Subtracting equation (A1) from (A2) and dividing by dy gives

$$\frac{d}{dy}(Q+U) = -\rho K_b(Q-U). \tag{A3}$$

Similarly, adding equations (A1) and (A2) and dividing by dy gives

$$\frac{d}{dy}(Q-U) = -\rho K_b(Q+U) + \rho K_b\alpha(Q+U). \tag{A4}$$

Let

$$R = Q + U \tag{A5}$$

$$T = Q - U. \tag{A6}$$

Substituting R and T in equations (A3) and (A4) yields

$$\frac{d}{dy}R = -T\rho K_b \tag{A7}$$

$$\frac{d}{dy}T = -\rho K_b R + \rho K_b\alpha R = -\rho K_b(1-\alpha)R. \tag{A8}$$

Differentiating equation (A8)

$$\frac{d^2}{d^2y}T = -\rho K_b(1-\alpha)\frac{dR}{dy}. \tag{A9}$$

Putting dR/dy from equation (A7) and rearranging equation (A9) yields

$$\frac{d^2}{d^2y}T - (\rho K_b)^2(1-\alpha)T = 0. \tag{A10}$$

Equation (A10) is a second-order linear ordinary differential equation that may be written in operational form as

$$(D-r)(D+r)T=0, \tag{A11}$$

where

$$D=\frac{d}{dy} \quad \text{and} \quad r=\rho K_b\sqrt{1-\alpha}. \tag{A12}$$

Denoting

$$(D+r)T=T_1, \tag{A13}$$

equation (A11) becomes

$$(D-r)T_1=0 \text{ or equivalently } \frac{dT_1}{dy}-rT_1=0. \tag{A14}$$

Equation (A14) is a first-order linear differential equation with solution

$$T_1=c_1\exp(ry). \tag{A15}$$

Putting T_1 in equation (A13) yields

$$(D+r)T=c_1\exp(ry) \quad \text{or equivalently} \quad \frac{dT}{dy}+rT=f_1(y), \tag{A16}$$

where

$$f_1(y)=c_1\exp(ry).$$

The solution to first-order linear differential equation (A16) is

$$\begin{aligned} T &= \exp(-ry)\int \exp(ry)f_1(y)dy + c_2\exp(-ry)\\ &= \exp(-ry)\int \exp(ry)c_1\exp(ry)dy + c_2\exp(-ry)\\ &= c_1\exp(-ry)\int \exp(2ry)dy + c_2\exp(-ry)\\ &= c_1\exp(-ry)\left[\frac{\exp(2ry)}{2r}+c_3\right] + c_2\exp(-ry)\\ &= \frac{c_1}{2r}\exp(ry) + c_1c_3\exp(-ry) + c_2\exp(-ry)\\ &= C_1\exp(ry) + C_2\exp(-ry). \end{aligned} \tag{A17}$$

This is the solution to equation (A10).

[62] Calculating R from equation (A8)

$$R=-\frac{1}{(1-\alpha)\rho K_b}\frac{dT}{dy}. \tag{A18}$$

Differentiating equation (A17), we get

$$\frac{dT}{dy}=C_1r\exp(ry)-C_2r\exp(-ry). \tag{A19}$$

Putting dT/dy in equation (A18)

$$\begin{aligned} R &= -\frac{1}{(1-\alpha)\rho K_b}[C_1r\exp(ry)-C_2r\exp(-ry)]\\ &= C_2\frac{r\exp(-ry)}{(1-\alpha)\rho K_b}-C_1\frac{r\exp(ry)}{(1-\alpha)\rho K_b} \end{aligned}. \tag{A20}$$

From equation (A5) and (A6), we have

$$Q=\frac{R+T}{2} \tag{A21}$$

$$U=\frac{R-T}{2}. \tag{A22}$$

Putting R and T in (A21) and (A22) gives $Q(y)$ and $U(y)$ as functions of depth y

$$\begin{aligned} Q(y) =& \frac{1}{2}\left[C_1\left(1-\frac{r}{(1-\alpha)\rho K_b}\right)\exp(ry)\right.\\ &\left.+C_2\left(1+\frac{r}{(1-\alpha)\rho K_b}\right)\exp(-ry)\right] \end{aligned} \tag{A23}$$

$$\begin{aligned} U(y) =& \frac{1}{2}\left[-C_1\left(\frac{r}{(1-\alpha)\rho K_b}+1\right)\exp(ry)\right.\\ &\left.+C_2\left(\frac{r}{(1-\alpha)\rho K_b}-1\right)\exp(-ry)\right]. \end{aligned} \tag{A24}$$

Substituting the value of r from equation (A12) in (A23) and (A24) yields

$$Q(y)=\frac{1}{2}\begin{bmatrix} C_1\left(1-\frac{1}{\sqrt{(1-\alpha)}}\right)\exp\left(\sqrt{(1-\alpha)}\rho K_b y\right)\\ +C_2\left(1+\frac{1}{\sqrt{(1-\alpha)}}\right)\exp\left(-\sqrt{(1-\alpha)}\rho K_b y\right)\end{bmatrix} \tag{A25}$$

$$U(y)=\frac{1}{2}\begin{bmatrix} -C_1\left(\frac{1}{\sqrt{(1-\alpha)}}+1\right)\exp\left(\sqrt{(1-\alpha)}\rho K_b y\right)\\ +C_2\left(\frac{1}{\sqrt{(1-\alpha)}}-1\right)\exp\left(-\sqrt{(1-\alpha)}\rho K_b y\right)\end{bmatrix}. \tag{A26}$$

Denoting $k'=\sqrt{(1-\alpha)}$ gives equations (10) and (11) in the body of the paper.

[63] **Acknowledgments.** We thank Jobie Carlisle, Robert Heinse and Justin Robinson for their help during the field work. We thank Martyn Clark, Jessica Lundquist and an anonymous WRR reviewer for their comments which significantly improved this manuscript. This research was supported by the USDA-CREES UT drought management project award 2008-34552-19042. This support is gratefully acknowledged.

References

Anderson, E. A. (1976), A point energy and mass balance model of a snow cover, *NOAA Tech. Rep. NWS* 19, U.S. Dept. of Commerce, Silver Spring, Md.

Bartlett, P., and M. Lehning (2002), A physical SNOWPACK model for the Swiss avalanche warning: Part I: numerical model, *Cold. Reg. Sci. Technol.*, *35*(3), 123–145, doi:10.1016/s0165-232x(02)00074-5.

Bonan, G. B. (1991), A biophysical surface energy budget analysis of soil temperature in the boreal forests of interior Alaska, *Water Resour. Res.*, *27*(5), 767–781.

Bristow, K. L., and G. S. Campbell (1984), On the relationship between incoming solar radiation and the daily maximum and minimum temperature, *Agr. Forest Meteorol.*, *31*, 159–166.

Dickinson, R. E. (1983), Land surface processes and climate-surface albedos and energy balance, *Adv. Geophys.*, *25*, 305–353.

Ellis, C. R., and J. W. Pomeroy (2007), Estimating sub-canopy shortwave irradiance to melting snow on forested slopes, *Hydrol. Processes*, *21*(19), 2581–2593, doi:10.1002/hyp.6794.

Essery, R., J. Pomeroy, J. Parviainen, and P. Storck (2003), Sublimation of snow from coniferous forests in a climate model, *J. Clim.*, *16*, 1855–1864.

Essery, R., P. Bunting, A. Rowlands, N. Rutter, J. Hardy, R. Melloh, T. Link, D. Marks, and J. Pomeroy (2008), Radiative transfer modeling of a coniferous canopy characterized by airborne remote sensing, *J. Hydrometeorol.*, *9*(2), 228–241, doi:10.1175/2007jhm870.1.

Fassnacht, K. S., S. T. Gower, M. D. MacKenzie, E. V. Nordheim, and T. M. Lillesand (1997), Estimating the leaf area index of North Central Wisconsin forests using the landsat thematic mapper, *Remote Sens. of Environ.*, *61*(2), 229–245, doi:10.1016/s0034-4257(97)00005-9.

Flerchinger, G. N., and Q. Yu (2007), Simple expressions for radiation scattering in canopies with ellipsoidal leaf angle distribution, *Agr. Forest Meteorol.*, *144*, 230–235.

Flerchinger, G. N., W. Xiao, T. J. Sauer, and Q. Yu (2009), Simulation of within-canopy radiation exchange, *NJAS–Wagen. J. Life Sc.*, *57*(1), 5–15, (http://www.sciencedirect.com/science/article/pii/S1573521409000062).

Goudriaan, J. (1977), Crop micrometeorology: A simulation study, simulation monographs, Cent. for Agric. Publ. and Doc., Wageningen, Netherlands.

Hardy, J. P., R. Melloh, P. Robinson, and R. Jordan (2000), Incorporating effects of forest litter in a snow process model, *Hydrol. Processes*, *14*(18), 3227–3237, doi:10.1002/1099-1085(20001230)14:18<3227::AID-HYP198>3.0.CO;2-4.

Hardy, J. P., R. Melloh, G. Koenig, D. Marks, A. Winstral, J. W. Pomeroy, and T. Link (2004), Solar radiation transmission through conifer canopies, *Agr. Forest Meteorol.*, *126*(3–4), 257–270.

Hedstrom, N. R., and J. W. Pomeroy (1998), Measurements and modelling of snow interception in the boreal forest, *Hydrol. Processes*, *12*(10–11), 1611–1625.

Hu, L., B. Yan, X. Wu, and J. Li (2010), Calculation method for sunshine duration in canopy gaps and its application in analyzing gap light regimes, *For. Ecol. Manag.*, *259*(3), 350–359, doi:10.1016/j.foreco.2009.10.029.

Jordan, R. (1991), A one-dimensional temperature model for a snow cover, *Tech. Doc. SNTHERM 89, Spec. Tech. Rep. 91-16*, U. S. Army Cold Reg. Res. and Eng. Lab., Hanover, N.H.

Koivusalo, H. (2002), Process-oriented investigation of snow accumulation, snowmelt and runoff generation in forested sites in finland, Ph.D. thesis, Helsinki Univ. of Technol., Helsinki, Finland.

Lehning, M., P. Bartelt, B. Brown, and C. Fierz (2002), A physical SNOWPACK model for the Swiss avalanche warning: Part III: Meteorological forcing, thin layer formation and evaluation, *Cold. Reg. Sci. Technol.*, *35*(3), 169–184, doi:10.1016/s0165-232x(02)00072-1.

Li, X., A. Strahler, and C. E. Woodcock (1995), A hybrid geometric optical-radiative transfer approach for modeling albedo and directional reflectance of discontinuous canopies, *IEEE T. Geosci. Remote*, *33*(2), 466–480.

Link, T., and D. Marks (1999), Distributed simulation of snowcover mass- and energy-balance in the boreal forest, *Hydrol. Processes*, *13*, 2439–2452.

Link, T. E., D. Marks, and J. P. Hardy (2004), A deterministic method to characterize canopy radiative transfer properties, *Hydrol. Processes*, *18*(18), 3583–3594, doi:10.1002/hyp.5793.

Luce, C. H., and D. G. Tarboton (2010), Evaluation of alternative formulae for calculation for surface temperature in snowmelt models using frequency analysis of temperature observations, *Hydrol. Earth Syst. Sci.*, *14*, 535–543.

Marks, D., J. Dozier, and R. E. Davis (1992), Climate and energy exchange at the snow surface in the alpine region of the Sierra Nevada, I: Meteorological measurements and monitoring, II: Snowcover energy balance, *Water Resour. Res.*, *28*(11), 3029–3054.

Meador, W., and W. R. Weaver (1980), Two-stream approximations to radiative transfer in planetary atmospheres: A unified description of existing methods and a new improvement, *J. Atmos. Sci.*, *37*, 630–643.

Monteith, J. L., and M. H. Unsworth (1990), *Principles of Environmental Physics*, 2nd ed., 289 pp., Edward Arnold, London.

Ni, W., X. Li, C. E. Woodcock, J.-L. Roujean, and R. E. Davis (1997), Transmission of solar radiation in boreal conifer forests: Measurements and models, *J. Geophys. Res.*, *102*(D24), 29,555–29,566, doi:10.1029/97jd00198.

Nijssen, B., and D. P. Lettenmaier (1999), A simplified approach for predicting shortwave radiation transfer through boreal forest canopies, *J. Geophys. Res.*, *104*(D22), 27,859–27,868

Niu, G.-Y., and Z.-L. Yang (2004), Effects of vegetation canopy processes on snow surface energy and mass balances, *J. Geophys. Res.*, *109*(D23), D23111, doi:10.1029/2004JD004884.

Norman, J. M. (1979), Modeling the complete crop canopy, in *Modification of the Arial Environment of Plants*, edited by B. J. Barfield and J. F. Gerber, pp. 249–277, Am. Soc. of Agric. and Biol. Eng., St. Joseph, Mich.

Price, A. G., and T. Dunne (1976), Energy balance computations of snowmelt in a subarctic area, *Water Resour. Res.*, *12*(4), 686–694.

Roujean, J.-L. (1996), A tractable physical model of shortwave radiation interception by vegetative canopies, *J. Geophys. Res.*, *101*(D5), 9523–9532, doi:10.1029/96jd00343.

Running, S. W., R. R. Nemani, D. L. Peterson, L. E. Band, D. F. Potts, L. L. Pierce, and M. A. Spanner (1989), Mapping regional forest evapotranspiration and photosynthesis by coupling satellite data with ecosystem simulation, *Ecology*, *70*(4), 1090–1101.

Satterlund, D. R. (1979), An improved equation for estimating long-wave radiation from the atmosphere, *Water Resour. Res.*, *15*, 1643–1650.

Sellers, P. J. (1985), Canopy reflectance, photosynthesis and transpiration, *Int. J. Remote Sens.*, *6*, 1335–1372.

Shuttleworth, W. J. (1993), Evaporation, in *Handbook of Hydrology*, edited by D. R. Maidment, pp. 4.1–4.53, McGraw-Hill, New York.

Stähli, M., T. Jonas, and D. Gustafsson (2009), The role of snow interception in winter-time radiation processes of a coniferous sub-alpine forest, *Hydrol. Processes*, *23*(17), 2498–2512, doi:10.1002/hyp.7180.

Storck, P., D. P. Lettenmaier, and S. M. Bolton (2002), Measurement of snow interception and canopy effects on snow accumulation and melt in a mountainous maritime climate, Oregon, United States, *Water Resour. Res.*, *38*(11), 1223, doi:10.1029/2002WR001281.

Tarboton, D. G., and C. H. Luce (1996), Utah energy balance snow accumulation and melt model (UEB), in *Computer Model Technical Description and Users Guide*, Utah Water Research Laboratory and USDA Forest Service Intermountain Research Station, Logan, Utah, 64 p. Available at http://www.engineering.usu.edu/dtarb/.

Tarboton, D. G., T. G. Chowdhury, and T. H. Jackson (1995), A Spatially Distributed Energy Balance Snowmelt Model, in Biogeochemistry of Seasonally Snow-Covered Catchments (Proceedings of a Boulder Symposium, July 1995), edited by K. A. Tonnessen, et al., IAHS Publ. no. 228, Wallingford, p. 141–155.

Tribbeck, M. J., R. J. Gurney, E. M. Morris, and D. W. C. Pearson (2004), A new Snow-SVAT to simulate the accumulation and ablation of seasonal snow cover beneath a forest canopy, *J. Glaciol.*, *50*, 171–182, doi:10.3189/172756504781830187.

U.S. Army Corps of Engineers (1956), Snow hydrology, summary report of the snow investigations, U.S. Army Corps of Engineers, North Pacific Division, Portland, Or.

Wigmosta, M. S., L. W. Vail, and D. P. Lettenmaier (1994), A distributed hydrology-vegetation model for complex terrain, *Water Resour. Res.*, *30*(6), 1665–1679.

Yang, R., M. A. Friedl, and W. Ni (2001), Parameterization of shortwave radiation fluxes for nonuniform vegetation canopies in land surface models, *J. Geophys. Res.*, *106*(D13), 14,275–14,286, doi:10.1029/2001JD900180.

You, J. (2004), Snow hydrology: The parameterization of subgrid processes within a physically based snow energy and mass balance model, Ph.D. thesis, Utah State University, Logan, Utah.

Zhao, W., and R. J. Qualls (2005), A multiple-layer canopy scattering model to simulate shortwave radiation distribution within a homogeneous plant canopy, *Water Resour. Res.*, *41*, W08409, doi:10.1029/2005WR004016.

Zhao, W., and R. J. Qualls (2006), Modeling of long-wave and net radiation energy distribution within a homogeneous plant canopy via multiple scattering processes, *Water Resour. Res.*, *42*, W08436, doi:10.1029/2005WR004581.

Zheng, G., and L. M. Moskal (2009), Retrieving leaf area index (LAI) using remote sensing: Theories, methods and sensors, *Sensors*, *9*(4), 2719–2745.

V. Mahat and D. G. Tarboton, Department of Civil and Environmental Engineering, Utah Water Research Laboratory, Utah State University, 4110 Old Main Hill, UT 84322-4110, Logan, USA. (vinod.mahat@aggiemail.usu.edu; dtarb@usu.edu)